

# Study on an Advanced Attitude Determination Algorithm for the ERG Spacecraft

By Halil Ersin SÖKEN, Shin-ichiro SAKAI,  
Kazushi ASAMURA, Yosuke NAKAMURA and Takeshi TAKASHIMA

*Institute of Space and Astronautical Science, JAXA, Sagami-hara, Japan*

JAXA's Arase Spacecraft, which is formerly known as Exploration of Energization and Radiation in Geospace (ERG), was launched on 20 December 2016. The spacecraft is spin-stabilized. Its mission is exploring how relativistic electrons in the radiation belts are generated during space storms. Two on-ground attitude determination algorithms are considered for the mission: a conventional simple algorithm that inherits from old missions and an advanced algorithm that is newly designed. This paper discusses the design of the advanced attitude determination algorithm. The algorithm is composed of three main parts: the coarse attitude estimator, star identification and tracking algorithm, and the fine attitude estimator. In this paper, we present the essentials of each algorithm and describe how they are put together to form the advanced attitude determination suite for Arase.

**Key Words:** ERG, Arase, Spinning Spacecraft, Attitude Determination

## 1. Introduction

JAXA's Arase spacecraft was launched on 20 December 2016. It is a small satellite mission into geospace which especially focuses on the relativistic electron acceleration as well as the dynamics of the space storms<sup>1)</sup>. High-energy particles (ions and electrons) are trapped in the Earth's magnetic field and formed the Van Allen radiation belts. The mission's aim is to elucidate acceleration and loss mechanisms of these highly-charged particles in the inner magnetosphere during space storms.

Along with these scientific interests studying the relativistic electrons in the radiation belts is important for the space weather<sup>1,2)</sup>. Spacecraft such as GPS and meteorological satellites operate in the radiation belts. Human space activities related to the International Space Station also take place at an altitude close the inner radiation belt. The high-energy particles can cause operational anomalies for the satellites and exert a dangerous impact on the mankind's long-term stay in space. Therefore a study on radiation belts is a requirement not just for current space activities but also for future missions.

Arase is Sun-oriented and spin-stabilized with  $\sim 7.5$ rpm spin rate. It weighs about 350kg. The spacecraft is located on a highly elliptical orbit with a perigee about 300km and an apogee about 30000km. It has four solar panels, two 5m long masts and four 15m long wire antennas which introduce flexibility to the overall spacecraft structure (Fig.1).

Two on-ground attitude determination algorithms are used for the mission: a conventional simple algorithm that inherits from old JAXA missions and an advanced algorithm that is newly designed. This paper discusses the design of the advanced attitude determination algorithm. We present each algorithm that composes the overall attitude determination suite and describe how these algorithm are integrated to estimate the spacecraft's attitude.

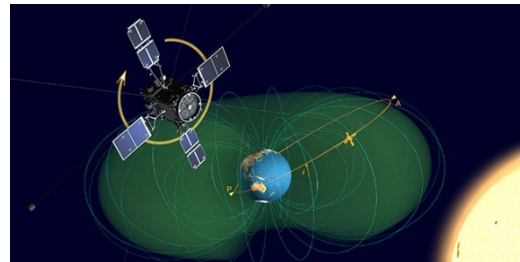


Fig. 1. Arase and its orbit (courtesy of ISAS/JAXA).

## 2. The Attitude Determination Suite Overview

Arase has three types of attitude sensors onboard (Fig.2): a three-axis fluxgate magnetometer (termed as Geomagnetic Aspect Sensor - GAS), two spin-type Sun aspect sensors (SSAS) and a star scanner (SSC). Only one of the SSASs is operational during the nominal mission.

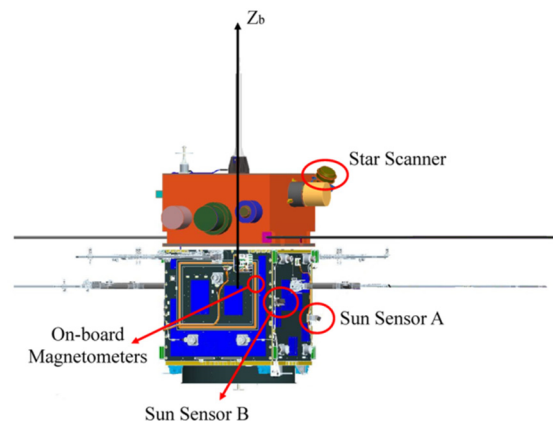


Fig. 2. Attitude sensors

The proposed attitude determination suite for the spacecraft is composed of three main parts: the coarse attitude estimator, star identification and tracking algorithm, and the fine attitude estimator (Fig.3). The coarse attitude estimation algorithm is

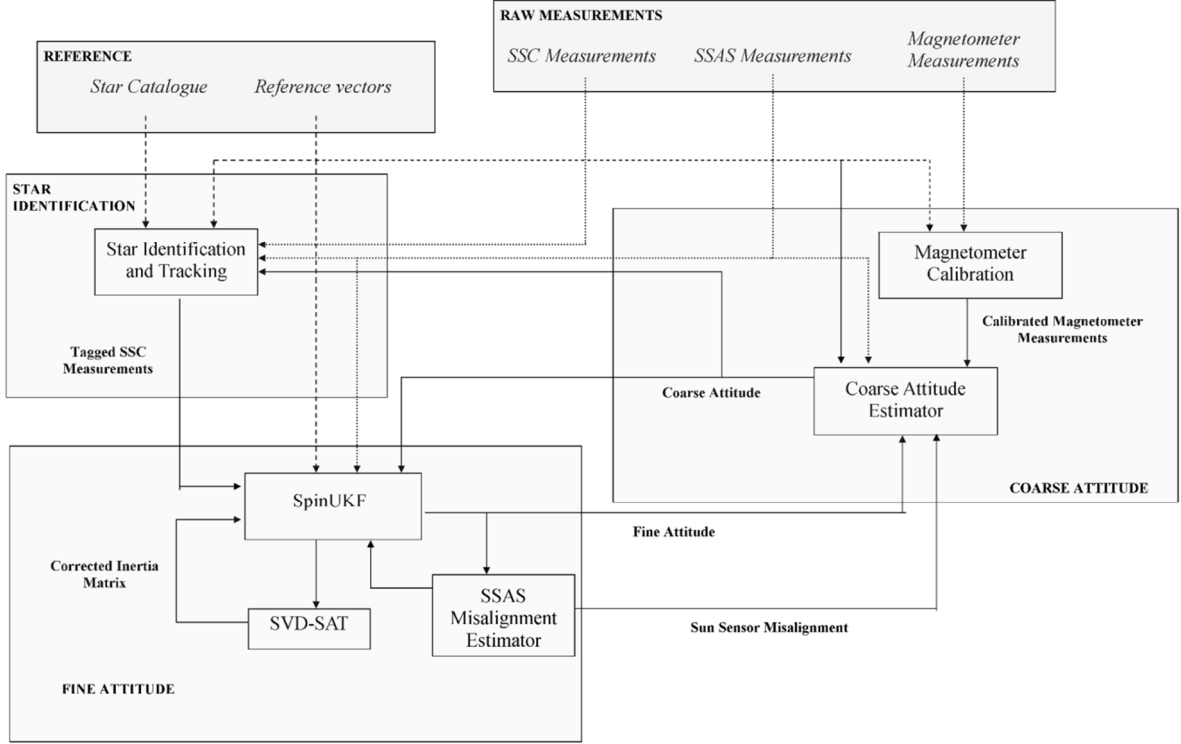


Fig. 3. Overview of the proposed attitude determination suite.

based on the GAS and SSAS measurements and uses different algorithms including the TRIAD and Tanygin-Shuster (T-S) algorithm<sup>3)</sup> to estimate a coarse spin-axis direction. The GAS measurements are calibrated using two different algorithms. The TWO-STEP algorithm<sup>4)</sup> is used for batch calibration. In the end, using the whole available GAS measurements, it provides single estimate for the vector of full calibration parameters: scale factors, nonorthogonality corrections and biases. The other magnetometer calibration algorithm, a pseudo-linear Kalman filter (PSLKF)<sup>5)</sup>, estimates the time-varying bias components, specifically over the perigee passes.

Once we have a coarse spin-axis direction estimate, we use this information to identify the star pulses detected by the SSC. The star identification algorithm first pairs the star pulses detected by the SSC and then uses the coarse attitude estimate to match the detected pulses with the catalogue stars. The identification process mainly uses a distance-orientation algorithm for star matching<sup>6)</sup>.

The fine attitude estimator consists of three algorithms: the Unscented Kalman Filter for spinning spacecraft (SpinUKF), the spin-axis tilt (SAT) estimation algorithm and the SSAS misalignment estimation algorithm. SpinUKF runs having so called spin parameters in its state vector and estimates the full three-axis attitude of the spacecraft along with the attitude rates, sequentially<sup>7)</sup>. Spin parameters consist of the spin-axis orientation unit vector in the inertial frame and the spin phase angle. This representation is advantageous as the spin axis direction components in the inertial frame do not change rapidly and the phase angle changes with a constant rate in the absence of a torque.

The SAT estimation algorithm estimates the SAT error, which is also known as dynamic imbalance or coning error. The algorithm is based on the Singular Value Decomposition (SVD) method<sup>8)</sup> and makes use of the attitude rates estimated by the SpinUKF. The SSAS misalignment estimation algorithm is also based on the SVD method and estimates the relative misalignment between the SSC and SSAS.

### 3. Coarse Attitude Estimation

Using the GAS and SSAS measurements a coarse attitude can be estimated for the spacecraft. This provides us the opportunity to know the spin-axis direction even when the SSC is turned off or when there is no visible/detected star. Moreover we use this coarse attitude estimate for star identification.

Before applying one of the methods for the coarse attitude estimation, the GAS is calibrated and its measurements are corrected.

#### 3.1. Magnetometer Calibration

The GAS is located onboard the Arase (Fig.2). Thus its measurements are corrupted with different errors caused by the nearby electronics and magnetic torquers (MTQs). We assume three types of errors are in effect for the GAS: bias, scale factors, and nonorthogonality.

The model for GAS measurements is,

$$\mathbf{B}_k = (\mathbf{I}_{3 \times 3} + \mathbf{D})^{-1} (\mathbf{A}_k \mathbf{H}_k + \mathbf{b}_k + \mathbf{v}_{m,k}), \quad (1)$$

where,  $\mathbf{B}_k$  is the magnetometer measurement vector,  $\mathbf{A}_k$  is the attitude matrix for the spacecraft, defining the attitude of the spacecraft body frame with respect to inertial frame,  $\mathbf{H}_k$

is the Earth's magnetic field in the inertial frame,  $D$  is a symmetric matrix with 6 parameters that reflect the scaling, nonorthogonality and soft iron errors,  $\mathbf{b}_k$  is the bias vector and  $\mathbf{v}_{m,k}$  is the the Gaussian zero-mean measurement noise with covariance  $\Sigma_k$  as  $\mathbf{v}_{m,k} \sim \mathcal{N}(0, \Sigma_k)$ .

### 3.1.1. Batch Calibration

Two different algorithms are run on-ground to correct the collected GAS measurements. The first of these is the TWO-STEP algorithm<sup>4)</sup>. It estimates a vector formed of 9 parameters: 3 for bias vector,  $\mathbf{b}_k$ , and 6 for the terms of the symmetric  $D$  matrix.

Essentially the TWO-STEP runs with a batch of GAS data collected over the first perigee pass of the spacecraft. The raw measurements,  $\mathbf{B}_{raw}$ , are corrected using the estimated bias vector,  $\hat{\mathbf{b}}$ , and  $\hat{D}$  matrix as,

$$\mathbf{B}_{cor} = (\mathbf{I}_{3 \times 3} + \hat{D}) \mathbf{B}_{raw} - \hat{\mathbf{b}}. \quad (2)$$

Assuming the estimated terms are not changing unless there is a change in the spacecraft configuration, the raw GAS data collected in the rest of the mission is corrected using the estimated parameters over the first perigee pass. Yet the TWO-STEP algorithm is run regularly to observe possible deviations in the estimated calibration parameters.

### 3.1.2. Real-time Magnetometer Calibration

Although the batch calibration algorithm is sufficient for coarse attitude estimation there are times that, specifically, the magnetometer bias terms vary. One of these cases is when the MTQ are activated about the perigee passes. Arase is a Sun-oriented spacecraft. The spacecraft is inertially stabilized and its spin-axis makes  $5^\circ \sim 15^\circ$  with the Sun direction. To correct  $\sim 1^\circ$ /day deviation of the spin-axis from this intended direction, the MTQs onboard the spacecraft are activated at certain perigee passes. This affects the GAS measurements and imposes additional biases.

The real-time magnetometer calibration algorithm, which is capable of sensing the time-variation in the bias terms, is essentially a Kalman Filter (KF) algorithm<sup>5)</sup>. The algorithm is an ordinary linear KF that operates on a linear model but the measurement matrix, which is given as

$$\begin{bmatrix} \tilde{b}_x \\ \tilde{b}_y \\ \beta \end{bmatrix} = \begin{bmatrix} 1 & 0 & 0 \\ 0 & 1 & 0 \\ 2B_x - b_x & 2B_y - b_y & 2B_z - b_z \end{bmatrix} \begin{bmatrix} b_x \\ b_y \\ b_z \end{bmatrix} + \begin{bmatrix} v_{mx} \\ v_{my} \\ \eta \end{bmatrix}, \quad (3)$$

is nonlinear. Therefore the algorithm is termed as the PSLKF. Here

$$\tilde{b}_{x,k} = \frac{1}{N} \sum_{i=k-N+1}^k B_{x,i} = b_{x,k} + v_{mx,k}, \quad (4a)$$

$$\tilde{b}_{y,k} = \frac{1}{N} \sum_{i=k-N+1}^k B_{y,i} = b_{y,k} + v_{my,k}. \quad (4b)$$

are measurements for the spin-planar bias terms that are formed using the spin-planar GAS measurements<sup>5)</sup>. The Gaussian white noise terms for these measurements are given as

$$v_{mx,k} = \frac{1}{N} \sum_{i=k-N+1}^k v_{mx,i}, \quad (5a)$$

$$v_{my,k} = \frac{1}{N} \sum_{i=k-N+1}^k v_{my,i}. \quad (5b)$$

The third and last measurement is

$$\beta_k = \|\mathbf{B}_k\|^2 - \|\mathbf{H}_k\|^2 = 2\mathbf{B}_k \cdot \mathbf{b}_k - \|\mathbf{b}_k\|^2 + \eta_k. \quad (6)$$

Here,

$$\eta_k = 2(\mathbf{B}_k - \mathbf{b}_k) \cdot \mathbf{v}_{m,k} + \|\mathbf{v}_{m,k}\|^2. \quad (7)$$

For the system equation in the PSLKF, the magnetometer bias terms are modeled as constant parameters,  $\dot{\mathbf{b}}_k = 0$ .

Notice that the real-time magnetometer calibration algorithm does not require attitude knowledge.

## 3.2. Coarse Attitude Estimation Algorithms

Once the GAS measurements are corrected, the coarse attitude of the spacecraft is determined using these measurements together with the SSAS measurements. The main algorithm that we use for coarse attitude estimation is TRIAD<sup>9,10)</sup>. The algorithm is implemented assuming that the SSAS measurements are more accurate compared to the GAS measurements.

As mentioned Arase has a highly elliptical orbit. The GAS measurements over and around the apogee are not usable for attitude determination. Thus we use the GAS measurements only over the perigee passes. The GAS measurements used in the coarse attitude estimation is limited such that  $|\mathbf{H}_k| > H_{per}$ ,

where  $H_{per} = 5000\text{nT}$  is the defined threshold for the magnitude of the reference magnetic field.

To confirm the validity of the TRIAD estimates, the attitude is also estimated by the T-S algorithm<sup>3)</sup>. The measurement model for the algorithm is defined as

$$\begin{bmatrix} B_z / \|\mathbf{B}\| \\ S_z \end{bmatrix} = \begin{bmatrix} \mathbf{H}^T \\ \mathbf{L}^T \end{bmatrix} \mathbf{1}_i^{spin} + \begin{bmatrix} v_{mz} \\ v_{sz} \end{bmatrix}. \quad (8)$$

Here  $B_z$  and  $S_z$  are body  $Z$  axis (spin-axis) measurements by the GAS and SSAS, respectively,  $\mathbf{L}$  is the sun direction vector in the inertial frame,  $\mathbf{1}_i^{spin}$  is the unit spin-axis vector, which is to be estimated, and  $v_{mz}$  and  $v_{sz}$  are the Gaussian white noise terms for the GAS and SSAS measurements.

The T-S algorithm may be run also using only the GAS measurements. However in this case measurements over a long period, including the apogee pass of the spacecraft, is needed.

## 4. Star Identification and Tagging

Star pulses detected by the SSC must be identified (matched with the catalogue stars) before using them as measurements.

The overall identification process is composed of star pulse pairing, identification and pulse tagging.

#### 4.1. Pairing

Pairing is the initial step of the star identification process. SSC pulses for 10 consecutive spin periods are paired as a single pulse for the same star with the pairing process. Pulses are paired with their initial detection if the detection time between two pulses is

$$\left| (t_{l,k+1}^{ssc} - t_{l,1}^{ssc}) - k \times P_{spin} \right| < \xi, \quad (9)$$

where  $P_{spin}$  is the spin period,  $t_{l,1}^{ssc}$  is the first detection time for the  $l^{th}$  pulse within one spin period and  $k$  is the spin no as  $k=1\dots9$ . The threshold value,  $\xi$ , is kept small as  $\xi=0.005s$  regarding the accurate SSC timing. The spin period is estimated using the mean of  $\omega_z^{ssas}$ , which is the spin rate measured by the SSAS as,

$$\omega_z^{ssas} = \frac{2\pi}{t_{k+1}^{ssas} - t_k^{ssas}} + v_{st}. \quad (10)$$

Here  $t_{k+1}^{ssas}$  and  $t_k^{ssas}$  are two consecutive Sun crossing times detected by the SSAS. The measurements are corrupted with zero-mean white noise  $v_{st}$  that depends on the Sun-sensor timing error.

The pairing for a pulse is accepted successful if the same pulse is detected for more than " $N$ " times within 10 spin periods. " $N$ " is set according to the user preference and the default value is 8.

During the pairing process the star direction in the inertial frame is also calculated (the unit star direction vector measured in the body frame is transformed to the inertial frame) using the coarse attitude information. For a set of paired pulses the mean of this unit star direction vector in the inertial frame is taken; in the identification process this mean value is used. Also the pulse magnitude values ( $V_{mag}$ ), which indicate the apparent magnitude for the stars, are averaged for paired star pulses at this phase.

There are two advantages of the pairing:

1) Misdetections within these 10 spin periods are removed and only valid star sightings are used in the identification process.

2) The random error for the SSC measurements increases at specific periods along the orbit (e.g. when the spacecraft is passing through the radiation belts). Also the coarse attitude estimate imposes random errors on the calculated unit star direction vectors in the inertial frame. By averaging the unit star direction vectors in the inertial frame, these random errors are minimized.

#### 4.2. Distance-Orientation Algorithm

The identification for the star pulses to match with the catalogue stars is performed based on the angular distance and orientation comparison for the star pairs. If there are more than one star detection, the algorithm first performs the comparison using only the star pairs and validates the identified stars using

Sun-to-star angular distances and orientations. On the other hand, if there is only one detected star, the Sun-to-star angular distances and orientations are compared.

The identification is performed using the vectors  $\vec{V}_c^{ij}$  in the catalogue (inertial) frame and  $\vec{V}_m^{kl}$  in the frame for the measurements. The frame for the measurements is the reflected inertial frame. It is formed by transforming the measurement vectors to the inertial frame using the coarse attitude estimates. These vectors are formed for each star (and the Sun) using the unit direction vectors (Fig.4),

$$\vec{V}_c^{ij} = \vec{1}_c^i - \vec{1}_c^j; \vec{V}_m^{kl} = \vec{1}_m^k - \vec{1}_m^l. \quad (11a,b)$$

After that the star identification is performed. The angular distances and cosine similarities (orientation) for each pairs are checked. If they satisfy certain conditions as,

$$\left| \|\vec{V}_c^{ij}\| - \|\vec{V}_m^{kl}\| \right| \leq \varepsilon, \quad (12a)$$

$$\cos \vartheta = \frac{\vec{V}_c^{ij} \cdot \vec{V}_m^{kl}}{\|\vec{V}_c^{ij}\| \|\vec{V}_m^{kl}\|} \geq 1 - \Delta, \quad (12b)$$

where  $\varepsilon$  and  $\Delta$  are the threshold values, than pulses  $i$  and  $j$  are identified as stars  $k$  and  $l$  from the catalogue, respectively. Note that if  $-\cos \vartheta \geq 1 - \Delta$  then pulse  $i$  is star  $l$  and pulse  $j$  is star  $k$ , instead. Once the stars are identified they need to be verified using the Sun-to-star angular distances and orientations calculated for each available star pulse in a similar manner. In this the unit direction vectors for one of the stars in Eq.11 is replaced by the Sun direction vector.

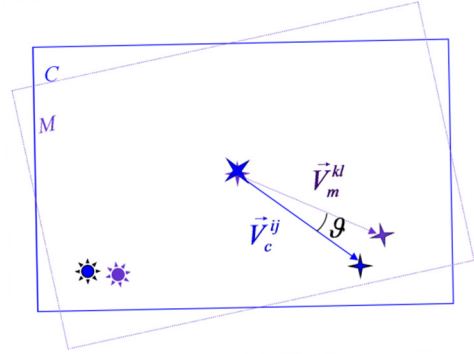


Fig.4. Star identification representation in 2D. M is the frame for the measurements and C is the catalogue (inertial) frame.

The threshold values for the identification algorithm,  $\varepsilon$  and  $\Delta$ , should be selected regarding various factors, including the accuracy of the coarse attitude estimate. So they may vary for each telemetry dataset. Yet in general threshold for orientation,  $\Delta$ , is smaller than the threshold for the angular distance,  $\varepsilon$ . In addition, to make the algorithm more robust, threshold values for the Sun-to-star validation phase are selected separately and are much smaller than those for star-to-star matching.

The magnitudes ( $V_{mag}$ ) of the star pulses are not directly used as a part of the identification process due to inaccuracy of these measurements. However, in case there is more than one

star detections the algorithm can verify if  $\left\|V_{mag}^i - V_{mag}^j\right| - \left|V_{mag}^k - V_{mag}^l\right| \leq \zeta$ , where  $\zeta$  is magnitude threshold set as 0.2.

### 4.3. Star Tagging

Once the paired star pulses are identified and matched with the catalogue stars, the pulses in the rest of the received SSC telemetry data are tagged with the identified star information. The tagging uses the timing information and checks if the pulse times are same - within a threshold - in a spin period. A pulse at  $k^{th}$  spin is tagged as one of the identified stars if it satisfies the condition

$$\left| \left( t_{i,k}^{ssc} - k \times P_{spin} \right) - \left( t_{i,i}^{ssc} - i \times P_{spin} \right) \right| < \xi, \quad (13)$$

for more than “ $N$ ” times with an already tagged pulse within the last 10 spin periods as  $i = (k-10) \dots (k-1)$ . The time threshold for tagging is same as the one for the pairing. Number of occurrence for condition (13) to tag a star, “ $N$ ” is selected by the user as  $N = 1 \dots 10$ .

## 5. Fine Attitude Estimation

Fine attitude estimation block of the proposed advanced attitude determination suite is used to get final attitude estimates for Arase based on the SSC and SSAS measurements. These fine attitude estimates are used while evaluating the science data. The block is composed of the SpinUKF, an attitude filter that estimates the spin axis direction and attitude rates, the SVD-SAT algorithm for estimating the SAT error and an algorithm for SSAS misalignment correction.

### 5.1. SpinUKF

The SpinUKF is essentially an UKF with the following state components: the spin-axis unit-vector direction terms  $\mathbf{1}_i^{spin} = [x \ y \ z]^T$  in the inertial frame, the spin-phase angle  $\gamma$ , and the body angular rate vector  $\boldsymbol{\omega}$  with respect to the inertial frame,

$$\mathbf{X} = [x \ y \ z \ \gamma \ \boldsymbol{\omega}]^T. \quad (14)$$

The UKF is derived for discrete-time nonlinear equations, so the system model is given by:

$$\mathbf{X}_{k+1} = \mathbf{f}(\mathbf{X}_k, k) + \mathbf{w}_k, \quad (15a)$$

$$\mathbf{Y}_k = \mathbf{h}(\mathbf{X}_k, k) + \mathbf{v}_k. \quad (15b)$$

Here,  $\mathbf{X}_k$  is the state vector and  $\mathbf{Y}_k$  is the measurement vector at time  $t_k$ . Moreover,  $\mathbf{w}_k$  and  $\mathbf{v}_k$  are the process and measurement error noises, which are assumed to be Gaussian white noises with covariance matrices  $\mathbf{Q}(k)$  and  $\mathbf{R}(k)$ , respectively. We estimate the inertial attitude of the spacecraft while the process is propagated by using the discrete-time versions of,

$$\dot{x} = \left( \frac{xzs(\gamma) + yc(\gamma)}{r} \right) \omega_x + \left( \frac{xzc(\gamma) - ys(\gamma)}{r} \right) \omega_y, \quad (16a)$$

$$\dot{y} = \left( \frac{yzs(\gamma) - xc(\gamma)}{r} \right) \omega_x + \left( \frac{yzc(\gamma) + xs(\gamma)}{r} \right) \omega_y, \quad (16b)$$

$$\dot{z} = -rs(\gamma)\omega_x - rc(\gamma)\omega_y, \quad (16c)$$

$$\dot{\gamma} = \omega_z - \frac{z}{r} (s(\gamma)\omega_y + c(\gamma)\omega_x), \quad (16d)$$

and the Euler’s dynamics equation which is required in the absence of gyros,

$$\dot{\boldsymbol{\omega}} = \mathbf{J}^{-1} [\mathbf{N} - \boldsymbol{\omega} \times (\mathbf{J}\boldsymbol{\omega})]. \quad (17)$$

Here  $c(\cdot)$  and  $s(\cdot)$  are  $\cos(\cdot)$  and  $\sin(\cdot)$  functions,

respectively,  $r = \sqrt{x^2 + y^2}$ ,  $\mathbf{J}$  is the inertia matrix of the spacecraft and  $\mathbf{N}$  is the torque vector, which is sum of the external disturbance torques such as solar radiation pressure and control torques, if there are any. For a detailed introduction and analyses of the SpinUKF the reader may refer to Ref. 7).

### 5.2. Spin-axis Tilt Estimation

The tilt error is observed as the mismatch between the actual spin axis that corresponds to the maximum principal axis of inertia, i.e. the principal  $Z$  axis (or  $-Z_p$ ) and the body  $Z$  axis (or  $-Z_b$ ), see Fig. 5, which is the intended spin axis during the design phase. The SAT can be represented as a rotation between the principal and body frames of the spacecraft and is described by the small Tait-Bryan angles,  $\theta_{cx}$  and  $\theta_{cy}$ . Assuming the rotation angles are small, the rotation matrix that transforms from the principal frame to the body frame is<sup>8)</sup>,

$$\mathbf{C}_{bp} = \begin{bmatrix} 1 & 0 & \theta_{cy} \\ 0 & 1 & -\theta_{cx} \\ -\theta_{cy} & \theta_{cx} & 1 \end{bmatrix}. \quad (18)$$

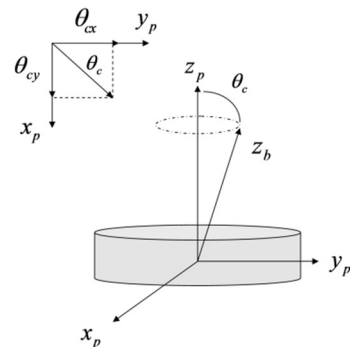


Fig.5. Spin-axis tilt (SAT).

The objective of the SVD-SAT algorithm is finding the rotation matrix which transforms the angular velocity vector in the body frame (estimated by the attitude filter) to the angular velocity vector in the principal frame. The spin rate around the

major principal axis is measured by the SSC using the time log for consecutive star crossings.

The cost function that is to be minimized using the SVD-SAT is

$$L(\theta_{cx}, \theta_{cy}) = \frac{1}{2} \sum_l a_l \left| \omega_p^l - \hat{C}_{pb}(\theta_{cx}, \theta_{cy}) \hat{\omega}_b^l \right|^2. \quad (19)$$

Here the hat operator denotes the estimated quantities,  $a_l$  is the sampling weight,  $\hat{\omega}_b^l = [\hat{\omega}_{bx}^l \ \hat{\omega}_{by}^l \ \hat{\omega}_{bz}^l]$  is the angular velocity vector in the body frame which is estimated by the SpinUKF filter and  $\omega_p^l$  is the angular velocity vector in the principal frame for the  $l^{\text{th}}$  measurement.  $\omega_p^l$  is given as,

$$\omega_p^l = [0 \ 0 \ \omega_z^{\text{SSC}}]^T. \quad (20)$$

$\omega_z^{\text{SSC}}$  is the spin rate of the spacecraft measured by the SSC, in a similar manner with (10).

For SAT estimation the SpinUKF is run using only the SSC measurements for a period when more than one star is detected by the SSC. The main reason is the higher accuracy of the SSC compared to the SSAS and the precaution for not being affected by possible SSAS misalignments. Note that the misalignment error here includes the effects for both the alignment errors for sensor's frame with respect to the spacecraft frame and sensor biases. In fact these two errors are indistinguishable for a spinning spacecraft<sup>11)</sup>. For the SSC we expect much lower combined sensor bias and misalignment error ( $\theta_\beta^{\text{SSC}} \cong 0.1^\circ$  for star aspect angle and  $\theta_\alpha^{\text{SSC}} < 0.045^\circ$  for azimuth at 7.5rpm spin rate) compared to those for the SSAS ( $\theta_\beta^{\text{SSAS}} \cong 0.5^\circ$  for Sun aspect angle and  $\theta_\alpha^{\text{SSAS}} \cong 0.11^\circ$  for azimuth at 7.5rpm spin rate).

The cost function (20) is minimized using the SVD method. The main advantage of the SVD over other algorithms is that it provides numerically robust solutions. The SVD method is well known<sup>12)</sup> so we do not present it here for brevity.

### 5.3. Sun sensor Misalignment Correction

Using the SpinUKF attitude estimates, the misalignment of the SSAS frame with respect to the SSC frame can be estimated. The cost function to be minimized is formulated as

$$L(\hat{C}_{ssas}) = \frac{1}{2} \sum_l b_l \left| \hat{C}_{ssas} \mathbf{S} - \hat{A}_l(x, y, z, \gamma) \mathbf{L} \right|^2, \quad (21)$$

where,  $\hat{C}_{ssas}$  is the misalignment matrix to be estimated and  $b_l$  is the sampling weight. Here we again use the SVD method to minimize the cost function and estimate the  $\hat{C}_{ssas}$  misalignment matrix. Note that SpinUKF is run using only the SSC measurements to estimate the attitude of the spacecraft,  $\hat{A}_l(x, y, z, \gamma)$ , when we apply the Sun sensor misalignment correction.

## 6. Conclusion

Details for an advanced attitude determination suite for JAXA's Arase (ERG) spacecraft were presented. Arase was launched on 20<sup>th</sup> December 2016. The proposed algorithms are being validated with the collected data from the spacecraft at the moment. The results will be presented in near future.

## Acknowledgments

This research is supported by the Arase (ERG) project of ISAS/JAXA.

## References

- 1) Takashima, T., Miyoshi, Y., Ono, T. and ERG project team: Geospace Exploration Mission ERG, 10<sup>th</sup> International Workshop on Radiation Effects on Semiconductor Devices for Space Applications, Tsukuba, Japan, JAXA-SP-12-008E, 2012.
- 2) Nagatsuma, T., Saito, S., Sakaguchi, K., Miyoshi, Y., Seki, K. and et.al: ERG Satellite Data Applied to Space Weather Forecasting, 29<sup>th</sup> International Symposium on Space Technology and Science, Nagoya, Japan, paper: 2013-r-44, 2013.
- 3) Tanygin, S. and Shuster, M.D.: Spin-Axis Attitude Estimation, *The Journal of the Astronautical Sciences*, **55:1**(2007), pp. 107-139.
- 4) Alonso, R. and Shuster, M.D.: TWOSTEP: A fast robust algorithm for attitude-independent magnetometer-bias determination, *The Journal of the Astronautical Sciences*, **50:4**(2002), pp. 433-451.
- 5) Soken, H.E. and Sakai, S.: Real-time Attitude-Independent Magnetometer Bias Estimation for Spinning Spacecraft, *Submitted: Journal of Guidance, Control, and Dynamics (under review)*.
- 6) Kosik, J.C.: Star Pattern Identification aboard an Inertially Stabilized Spacecraft, *Journal of Guidance, Control and Dynamics*, **14:2** (1991), pp.230-235.
- 7) Soken, H.E., Sakai, S., Asamura, K., Nakamura, Y. and Takashima, T.: Spin Parameters and Nonlinear Kalman Filtering for Spinning Spacecraft Attitude Estimation, 27<sup>th</sup> AAS/AIAA Space Flight Mechanics Meeting, San Antonio, TX, USA, AAS 17-249, 2017.
- 8) Soken, H.E., Sakai, S., Asamura, K., Nakamura, Y. and Takashima, T.: Spin-Axis Tilt Estimation for Spinning Spacecraft, AIAA Guidance, Navigation and Control Conference, AIAA 2016-0626, San Diego, USA, 2016.
- 9) Black, H.D: A Passive System for Determining the Attitude of a Satellite, *AIAA Journal*, **2:7**(1964), pp. 1350-1351.
- 10) Markley, F.L. and Crassidis, J.L.: *Fundamentals of Spacecraft Attitude Determination and Control*, Springer, New York, USA, 2014, pp.184-185.
- 11) Van der Ha, J.C.: Spin Axis Attitude Determination Accuracy Model in the Presence of Biases, *Journal of Guidance, Control, and Dynamics*, **29-4**(2006), pp.799-809.
- 12) Markley, F.L. and Crassidis, J.L.: *Fundamentals of Spacecraft Attitude Determination and Control*, Springer, New York, USA, 2014, pp.196-197.